Influence of degradation on the electrical conduction process in ZnO and SnO2-based varistors

M. A. Ponce, M. A. Ramírez, R. Parra, C. Malagú, M. S. Castro et al.

Additional information on J. Appl. Phys.

Influence of degradation on the electrical conduction process in ZnO and SnO$_2$-based varistors

M. A. Ponce,[1,a] M. A. Ramírez,[2] R. Parra,[1] C. Malagú,[3] M. S. Castro,[1] P. R. Bueno,[2] and J. A. Varela[2]

[1]*Institute of Materials Science and Technology (INTEMA) University of Mar del Plata and National Research Council (CONICET), Juan B. Justo 4302, B7608FDQ Mar del Plata, Argentina*
[2]*Institute of Chemistry, Universidade Estadual Paulista (UNESP), CEP 14800-900, Araraquara, Sao Paulo, Brazil*
[3]*Department of Physics, University of Ferrara, Via Saragat 1/c, 44100 Ferrara, Italy*

The conduction process during degradation, promoted by the application of fixed dc bias voltage at different temperatures (thermal steady states) and current pulses 8/20 μs on ZnO and SnO$_2$-based varistors, was studied comparatively in the present work. The electrical properties of the varistor systems were highly damaged after degradation with current pulse 8/20 μs. Variations on the potential barrier height and donor concentration were calculated by fitting the experimental data from impedance spectroscopy measurements assuming the formation of Schottky barriers at the grain boundaries and electrical conduction to occur due to tunneling and thermionic emission. © *2010 American Institute of Physics.* [doi:10.1063/1.3490208]

I. INTRODUCTION

Metal oxide varistors are electronic ceramic devices whose function is to sense and limit transient voltage surges and to do it so repeatedly without being destroyed or damaged. Their nonlinear current-voltage behavior is described by the equation $I = V^\alpha$, where α is the nonlinear coefficient whose magnitude is strongly influenced by the addition of transition metal oxides to the varistor composition.[1–3]

Since the first reports, tin dioxide varistors have demonstrated many advantages over the traditional ZnO varistors.[4] Due to the higher electrical breakdown fields, the former are suitable for high-voltage applications in the form of even smaller devices. Furthermore, they exhibit higher thermal conductivity than ZnO-based varistors, which is an advantage concerning stability toward thermal runaway. The microstructure consists in SnO$_2$ grains with atomic defects such as positively charged donors located at the depletion layers and negatively charged acceptors at grain boundaries.[3] Nevertheless, Glot pointed out some disadvantages of SnO$_2$ varistors such as the strong sensitivity to humidity and difficulties in attaining grains big enough for low voltage applications.[4,5]

The non-Ohmic conduction have the same physical nature in both (ZnO and SnO$_2$) systems associated with electron transport across voltage barriers located at the intergrain junctions.[6] However, different opinions exist regarding the conduction mechanisms and the thermionic model is mostly suggested to control conduction across Schottky-type voltage barriers.[7,8]

It is well known that, assuming that Schottky barriers are formed at the grain boundaries, the barrier height (ϕ), and donor density (N_d) are directly related as follows:

$$\phi = \frac{q^2 N_s^2}{2\varepsilon_r \varepsilon_0 N_d}, \tag{1}$$

where N_s is the number of electrons (per unit of area) extracted from the depleted surface region Λ, ε_0 the vacuum permittivity, ε_r the metal oxide relative permittivity, and q the electron charge. The usual Schottky relation between ϕ and Λ can be obtained from Eq. (1) considering that for a double Schottky (in a n type semiconductor) $2N_d = N_s$. The energy ϕ(eV) is the energy that the electrons must attain before they can move to surface energy level. Then, Λ can be deduced form Eq. (1) as follows:

$$\Lambda = \left(\frac{\varepsilon_0 \varepsilon_r \phi}{2q^2 N_d}\right)^{1/2}. \tag{2}$$

Then, assuming for example, $N_d = 10^{24}$ m^{-3}, $\phi = 0.95$ eV, and $\varepsilon_r = 10$ ($\varepsilon = \varepsilon_0 \cdot \varepsilon_r$) one notes that Λ is approximately 22 nm and for example $N_d = 5 \times 10^{24}$ m^{-3}, $\phi = 0.95$ eV, and $\varepsilon_r = 10$ ($\varepsilon = \varepsilon_0 \cdot \varepsilon_r$) then $\Lambda = 10$ nm. At this point it is important to note that the depletion layer region has been measured at the barrier bottom. Consequently, it is not always true that the maximum contribution to field emission is situated near the bottom of the barrier, indeed it can be situated near half barrier height as was explained in the work by Crowell and Rideout.[9] A fundamental aspect to consider is that (at the bottom of the barrier) the distance is higher and the density of electrons is exponentially higher too, due to the lower "distance" from the Fermi level (FL). Where, instead, the barrier is thin the density of electrons is very low because of the increased "distance" from FL. Consequently, it is not always true that the maximum contribution to field emission is situated near the top of the barrier, indeed it can be situated near-half barrier height, as shows Rhoederick and Williams.[10] Therefore, there is no difficulty in distinguish between the field emission contribution from the thermionic one, as explained Crowell's works.[9]

[a]Electronic mail: mponce@fi.mdp.edu.ar.

In this work, we studied the possible conduction mechanisms in SnO_2 and ZnO-based varistors before and after the electrical degradation by the application of a dc bias voltage at different temperatures and $8/20$ μs current pulses. Finally, thermionic (J_{therm}), tunneling (J_{tun}), and total current densities (J_{total}) are predicted in this work.

II. EXPERIMENTAL PROCEDURE

The ceramic varistor systems studied herein correspond to ZnO- and SnO_2-based systems. The traditional modified Matsuoka's system[11] in mol %: 95.4% $ZnO+1.5\%$ Sb_2O_3 $+1\%$ $NiO+0.1\%$ $SiO_2+0.5\%$ (Bi_2O_3, SnO_2, Co_2O_3, and MnO) [ZnO] and the Pianaro's system[12] 98.9% SnO_2 $+1\%$ $CoO+0.05\%$ $Nb_2O_5+0.05\%$ Cr_2O_3 [SnO_2], all values in mol %. The powders were prepared by the mixed oxide route and pressed uniaxially to obtain disks with adequate area/volume ratio.[13] ZnO-based samples were sintered at 1180 °C for 2 h and SnO_2-based samples were sintered at 1300 °C for 1 h. The apparent density of sintered samples was estimated by the Archimedes methodology and average grain sizes from scanning electron microscope images by means of interceptions method. A density value of the 99% comparatively to theoretical density of ZnO was measured for the zinc oxide sample, which showed 8.5 μm average grain size. The tin oxide sample showed a 98.5% of the theoretical density of cassiterite and an average grain size of 4.5 μm.

In order to compare the degradation behavior of ZnO- and SnO_2-based varistors, the same degradation processes were used for both ceramics. A dc bias voltage (corresponding to an electric field associated with a 0.05 $mA\ cm^{-2}$ current density) was applied to the sintered samples. The degradation process is accelerated by increasing the temperature from 50 to 200 °C for periods of 24 h (thermal steady-state conditions) under this continuous voltage level. The degradation occurs due to continuous leakage current that crosses the polycrystalline samples during the test. The leakage current was measured at intervals of 3 s (using a voltage source-measure unit Keithley 237). For each system, the aging stress was performed on three different samples to assure reproducibility. Also, the pulsed current degradation process was studied on different samples with adequate area/volume ratio by means of a high-voltage circuit based on three capacitors with a total capacitance of 2.25 μF and maximum voltage and energy of 200 kV and 45 kJ, respectively, used to generate $8/20$ μs current pulses. The corresponding electrical responses of the devices were registered with a Tektronix (8 bits, 100 MHz) digital oscilloscope. The encapsulation of ceramic disks must be carefully done since the selected material might influence the electrical response. In this work, the encapsulation was done according to the previously reported procedure.[14] The sample blocks of both systems were degraded by directly applying a series of individual current pulses with different magnitudes of current (from 100 A up to 5 kA) in the same conditions. The time between pulses was fixed at 20 s. For each sample a predetermined number of pulses were applied until either degradation occurred or the voltage wave fell down to null values.

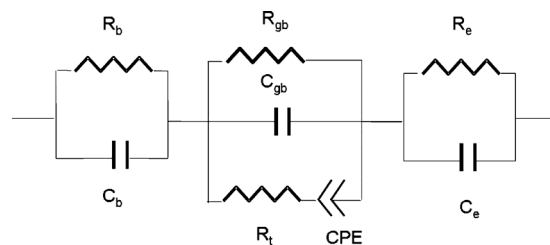Before and after the degradation process, each sample

FIG. 1. Electrical equivalent circuit used to model the electrical grain boundary resistance and capacitance.

was electrically characterized by current-voltage and impedance spectroscopy (IS) analyses. The electrical breakdown field (E_b), the nonlinearity coefficient (α) and the leakage current (I_L) were obtained from J-E curves. The measurements were carried out under room temperature conditions with a Keithley 237 source-measurement unit with a maximum current value of 10 mA. IS analyses were carried out using an HP4192 frequency response analyzer covering frequencies from 5 Hz to 110 MHz with a signal amplitude of 1 V. A continuous current potential (38 V dc bias) was also superimposed over the alternating potential in order to improve measurements and reduce possible residual noise. Curves of the imaginary ($-Z''$) versus the real (Z') component of impedance were fitted with a parallel RC circuit using the appropriated impedance software in order to obtain the grain boundary resistance (R_{gb}) and capacitance (C_{gb}). The electrical grain boundary resistance and capacitance were modeled using equivalent circuits previously proposed (Fig. 1). The grain boundary resistance (R_{gb}) and capacitance (C_{gb}) were obtained from theses analysis using the same methodology employed in Ref. 15.

III. RESULTS AND DISCUSSION

Figure 2 shows the J-E curves before and after the degradation treatments (dc-bias voltage and $8/20$ μs current pulses). Figure 2(a) shows the J-E curves for ZnO before and after the pulse and dc degradation treatments, and Fig. 2(b) shows the same kind of curves for SnO_2. In Table I we present the electrical parameters derived from these curves. Both ZnO- and SnO_2-based ceramics displayed the expected nonlinear behavior. The tin oxide varistor showed higher electric breakdown field (E_b) than the zinc oxide device. However, the most interesting results came out after the degradation treatment. Although the leakage current increased considerably for both systems, the E_r diminished 85% with respect to the initial value for ZnO and only 1% for SnO_2 for dc bias voltage degradation. This is in agreement with previous results on the higher resistance on SnO_2 ceramics to electrical degradation.[8]

Figure 3 shows the electrical capacitance and resistance curves for SnO_2-based varistors. In Fig. 3(a), curves obtained for the capacitance (C_p) before and after dc and pulse degradation processes for SnO_2 are presented and in Fig. 3(b) the electrical resistance (R_p) curves before and after degradation processes are shown. In Fig. 3(a) the C_{gb} before and after degradations can be obtained in the high frequency limit as it was previously explained.[15] Then,
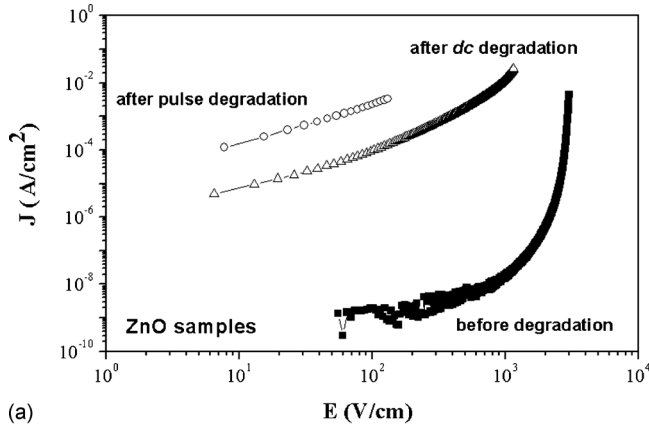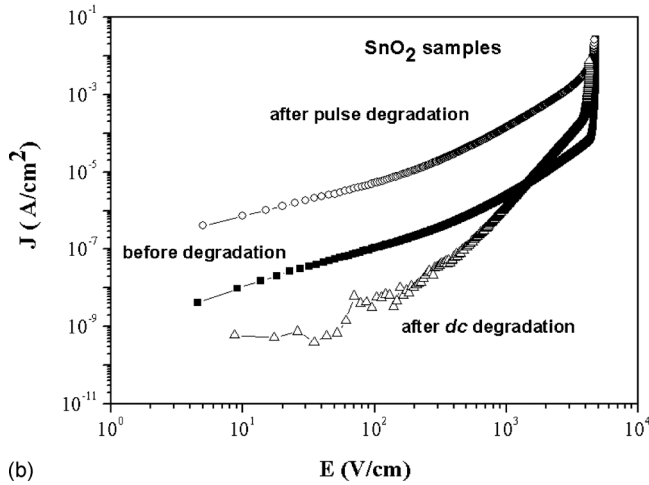
FIG. 2. Current density (J) vs electric field (E) curves before and after dc and pulse degradation. For ZnO (a) and SnO$_2$-based varistors (b).

FIG. 3. SnO$_2$-based varistors: (a) capacitance (Cp) before and after degradation process and (b) resistance (Rp) before and after degradation process.

$$C_p|_{\omega \to \infty} = C_{gb}. \tag{3}$$

On the other hand, in the limits of very low frequencies (at R_p versus frequency plots), R_{gb} can be determined as follows:
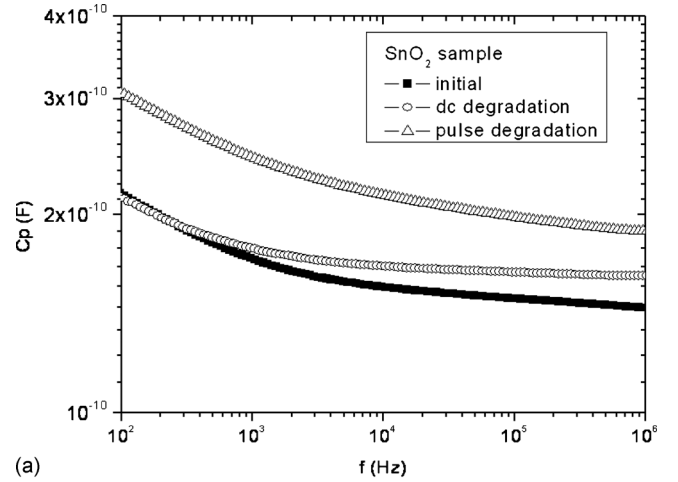
$$R_p|_{\omega \to 0} = R_{gb}, \tag{4}$$

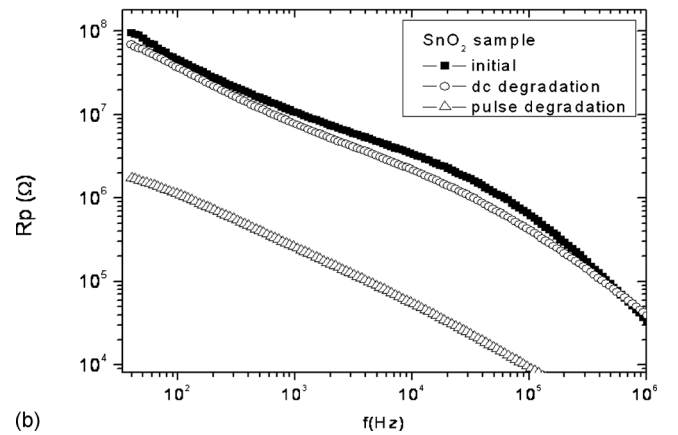where, C_{gb} was measured at frequencies above 100 kHz and R_{gb} below 100 Hz.

Figure 4 shows the C_p and R_p curves versus frequency for ZnO varistors, before and after dc and pulse degradations. In order to obtain the C_{gb} and the R_{gb} values, for ZnO-based varistors, the same methodologies showed previously for Figs. 3(a) and 3(b) were employed with the values obtained from Figs. 4(a) and 4(b). The obtained values are shown in Table II. It can be observed that while the sample resistance decreases during the samples degradation, the capacitance increases. We attribute this relationship, between resistance and capacitance changes, to the grain boundary barriers as was discussed in earlier studies.[15] After degradations, the experimental results showed a grain boundary resistance (R_{gb}) higher in more than an order of magnitude and, also, a lower capacitance (C_{gb}) that stands for a higher voltage barrier at grain boundaries. Assuming that all grains have the same size, that all barriers and the section of all grain boundaries are the same, this relationship is also related to the Schottky-type barrier height (ϕ) that is inversely proportional to the grain boundary capacitance and directly proportional to the donor concentration (N_d), Eq. (5) (Refs. 11 and 15)

$$\frac{1}{C_{gb}} = 2\left(\frac{2\phi n^2}{q^2 \varepsilon_0 \varepsilon_r N_d S^2}\right)^{1/2}, \tag{5}$$

where n is the average number of grains across the specimen thickness, ϕ is the barrier height (eV), q is the electron charge, ε_0 is the vacuum permittivity, ε_r is the metal oxide relative permittivity, and S is the area of the electrodes.[11]

If Schottky-type electrical barriers are assumed to exist at grain boundaries, the negative surface charge at the interface separating two grains is compensated by the positive

TABLE I. Electric breakdown field (E_b), leakage current (I_l), and nonlinearity coefficient (α).

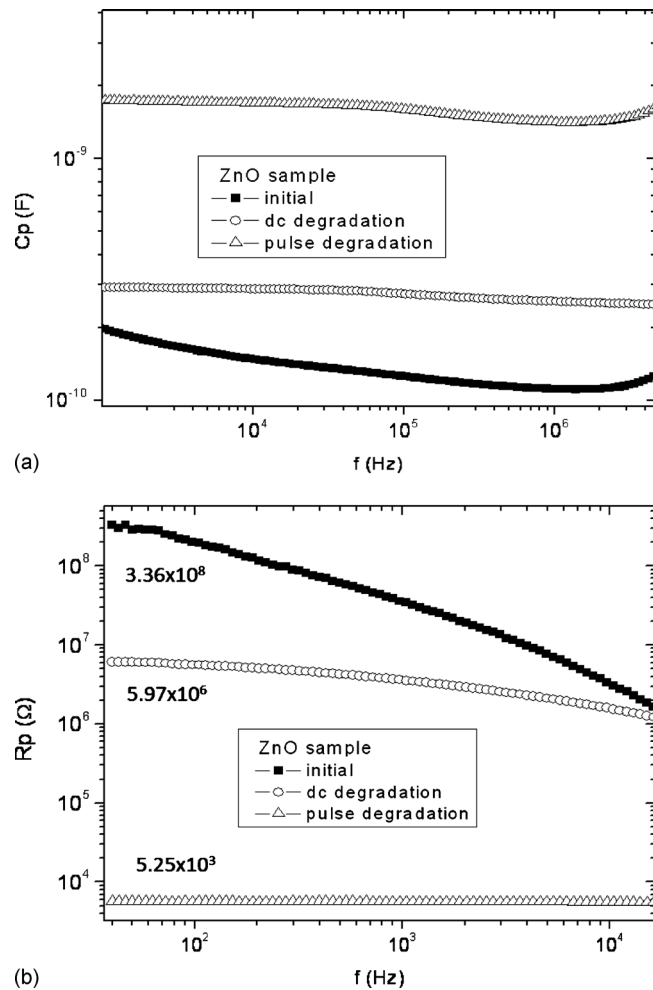| Sample	E_b (V/cm)	I_l (μA)	α
ZnO before	2610	3.7	68
ZnO dc	395	296	2
ZnO pulse	53	2620	1
SnO$_2$ before	4050	3.8	46
SnO$_2$ dc	4040	3.9	44
SnO$_2$ pulse	2590	235	4

FIG. 4. ZnO-based varistors: (a) capacitance (Cp) before and after degradation process and (b) resistance (Rp) before and after degradation process.

charge in the depletion layers in the grains on both sides of the interface.[15–17] This atomic defect model involves negatively charged acceptors (O′, O″ and V''_{Sn}, V'''_{Sn} for SnO$_2$ varistors and V'_{Zn}, V''_{Zn} for ZnO varistors) at the grain boundary interfaces and positively charged intrinsic donors ($V^{\bullet\bullet}_O$, $V^{\bullet}_O$ and $Zn^{\bullet}_i$, $Zn^{\bullet\bullet}_i$ for ZnO varistors) and extrinsic donors at the depletion layers. Deep negatively charged species at intergrains regions contribute to the potential barrier height. Indeed, positive donors in the depletion layers attract O′ and O″ species, among others, to the interface between adjacent grains, increasing the barrier height voltage and increasing

varistors behavior, assumption supported by the results obtained for the sintered sample in an enriched O$_2$ atmosphere.[18]

Now, we will focus on the electrical conduction mechanism. Several authors consider thermionic conduction as the dominant process in SnO$_2$ and ZnO varistors. In this work, we propose conduction due to a purely thermionic mechanism as a first approach. Assuming the purely thermionic mechanism contribution, values of barrier height were obtained using the corresponding current expression and the resistance at the grain boundary,

$$J = AT^2 \exp(-\phi/kT), \tag{6}$$

where A and k are the Richardson and Boltzmann constants and T the absolute temperature. The current density (J), of the ZnO and SnO$_2$-based varistors before and after degradation, can be obtained from the grain boundary resistance considering the following relationship:

$$J = V/SR_{gb}, \tag{7}$$

where V is the applied voltage during IS measurements, S the varistor area (3.85×10^{-5} m^2), and R_{gb} the grain boundary resistance for each varistor before and after degradations obtained from Figs. 3(b) and 4(b). Then using Eqs. (6) and (7) values of barrier height for varistors samples (before and after degradation) were obtained has follows:

$$\phi = -kT \ln(V/SR_{gb}AT^2). \tag{8}$$

After that, employing Eq. (5) and using the C_{gb} values obtained (for SnO$_2$ and ZnO-based varistors before and after degradation) from Figs. 3(a) and 4(a), respectively, the donor concentration values were calculated. For N_d estimation the relative permittivity (ε_r) values employed in Eq. (5) were 8.5 for ZnO and 14 for SnO$_2$ and a varistor area (S) of 3.85 $\times 10^{-5}$ m^2. Using this methodology, fitting values of barrier height and donor concentration (for SnO$_2$ and ZnO-based varistors) around 0.8 eV and 10^{23}–10^{24} m^{-3},[16,19] respectively, were obtained. The obtained values are shown in Table II in the columns titled "only thermionic conduction consideration." These values are in concordance with those reported by other authors.[18,19] However, changes in the electrical capacitances suggest that donor concentration do not remain constant. The aim of this work consists in evaluating the C_{gb} variation during the varistors dc bias voltage and current pulse degradations. Therefore, by means of the evalu-

TABLE II. Experimental C_{gb} and R_{gb}. The barrier height and width are shown as parameters obtained using the thermionic plus tunnel model.

Semiconductor oxide based varistor $S = 3.85 \times 10^{-5}$ m^2		R_{gb} (Ω)	C_{gb} (F)	ϕ (eV)	N_d (m^{-3})	ϕ (eV)	N_d (m^{-3})	Λ (nm)
		Grain boundary resistance	Grain boundary capacitance	Only thermionic conduction consideration		Thermionic plus tunnel estimation		
SnO$_2$, $\varepsilon r = 14$, $n = 455$	As sintered	9.9×10^7	1.5×10^{-10}	0.833	1.1×10^{23}	0.896	1.1×10^{24}	17.5
	dc	7.0×10^7	1.6×10^{-10}	0.824	1.2×10^{24}	0.896	1.3×10^{24}	16.5
	Pulse	1.8×10^6	1.9×10^{-10}	0.730	1.5×10^{24}	0.801	1.6×10^{24}	13.8
ZnO, $\varepsilon r = 8.75$, $n = 155$	As sintered	3.4×10^8	1.3×10^{-10}	0.864	1.5×10^{23}	0.922	1.6×10^{23}	37.7
	dc	6.0×10^6	2.5×10^{-10}	0.761	5.5×10^{23}	0.825	5.6×10^{23}	18.8
	Pulse	5.2×10^3	1.4×10^{-9}	0.580	1.3×10^{25}	0.771	1.7×10^{25}	3.3

ation of C_{gb} variation it was assumed that the conduction is composed by two main grain boundary conductive contributions, thermionic and tunneling, simultaneously. Then, tunneling through the barriers was included for a more accurate characterization of these polycrystalline semiconductor systems.[9,20] A reduction in the donor concentration, as determined from the experiments, naturally implies significant changes in the electrical response of the sample. If the change in capacitance were entirely due to a change in the barrier height, the associated grain boundary resistance would be smaller than the measured value.

The total current density over and through a barrier can be calculated as

$$J = \frac{AT}{k} \int_0^{V_s} f(E)P(E)dE + AT^2 \exp(-\phi/kT). \quad (9)$$

The first term corresponds to the tunneling current and the second to the thermionic current, A and k are the Richardson and Boltzmann constants, and $f(E)$ is the Fermi–Dirac distribution. $P(E)$, the transmission probability for a reverse-biased Schottky barrier (which is the limiting step, as was explained by Castro and Aldao[16]), is given by

$$P(E) = \left\{ \exp - \left[\frac{4\pi V_s}{qh} \left(\frac{m\varepsilon}{N_d} \right)^{1/2} \ln\left(1 - \frac{(1-\beta)^{1/2}}{\beta^{1/2}} \right) \right] \right\}, \quad (10)$$

where m is the electron effective mass, $\varepsilon (\varepsilon = \varepsilon_0 \cdot \varepsilon_r)$ is the electrical permittivity (8.5 for ZnO and 14 for SnO$_2$), h is the Planck constant, and β is E/ϕ.[21]

Using the calculated value of ϕ(eV) [obtained from grain boundary resistance measurements and the thermionic approximation, Eq. (8)] and the donor concentration value N_d(m^{-3}) [calculated from Eq. (5)] as initial pair of values and solving Eqs. (9) and (10), a first approach was done. After that, the total current result is greater than experimentally measured and calculated in with Eq. (6). A new pair of N_d and ϕ values was used for fitting experimental values with Eqs. (5), (9), and (10). Iterative calculations were carried out until the calculated total current (thermionic and tunnel current) was equal to the experimental value obtained with Eq. (6).

We found that, the barrier height is affected after degradation when an increase in C_{gb} is registered after each electrical stressing step (Table II). Actually, the variation in the capacitance is insufficient for the observed barrier height modifications. On the other hand, as mentioned above, the barrier characteristics are supposed to change due to ion, and oxygen vacancies migration that modify the donor concentration at depletion zones. The N_d value is seen to compensate the decrease in ϕ. Depending on the model used for fitting, different barrier height values are obtained. Generally, the simple thermionic conduction model gives lower barrier heights than the complete model (thermionic plus tunneling model). Finally, with the obtained values of N_d and ϕ from the tunneling plus thermionic approximation, the depletion layer region is calculated using Eq. (2).

Table III, shows the current densities predicted using thermionic (J_{therm}) and tunneling (J_{tun}) current models. These

TABLE III. Total experimental current densities (J_{total}) obtained using Eq. (7) and predicted thermionic (J_{therm}) and tunnel (J_{tun}) current densities. The sum from considering the thermionic plus tunnel conduction approaches the real value (J_{total}).

		Thermionic current densities (A/cm^2)	Thermionic plus tunneling current densities (A/cm^2)	
			J_{therm}	J_{tun}
SnO$_2$	As sintered	2.6×10^{-8}	1.1×10^{-8}	2.5×10^{-8}
	dc	3.7×10^{-8}	1.0×10^{-8}	2.8×10^{-8}
	Pulse	1.4×10^{-6}	4.1×10^{-7}	1.1×10^{-6}
ZnO	As sintered	7.7×10^{-9}	3.7×10^{-9}	3.6×10^{-9}
	dc	4.4×10^{-7}	1.6×10^{-8}	2.8×10^{-7}
	Pulse	4.9×10^{-4}	1.3×10^{-6}	4.5×10^{-4}

values are associated with the barrier height and donor concentration of Table II. For SnO$_2$-based varistors, tunneling conduction is, at least, the double of the thermionic current. It is observed that, after pulse degradation, tunnel current is three times greater than thermionic. The total current, is significantly tunnel current. It is known that variations in the grain size, dopants, and temperature exposure conditions of varistors results in different types of conduction phenomena. As in the case of SnO$_2$-based varistors, in ZnO varistors, the tunnel and thermionic conductions have the same weight before degradation. In this condition thermionic conduction cannot be neglected. In contrast, with the SnO$_2$-based varistor, after the dc degradation process, tunneling conduction overcomes thermionic conduction in one order of magnitude. The calculated values of currents presented in Table III, for ZnO pulse degradation, show that tunneling conduction is two orders of magnitude greater than the thermionic conduction and the total current is basically due to tunneling conduction. In this case, barriers are completely degraded and depletion layer was found to be 3.3 nm. For ZnO samples it is also possible to observe that the electrical properties remain permanently degraded. A similar experiment was performed with the SnO$_2$ samples which showed a greater resistance to degradation. The R_{gb} decreased only 15% after being exposed to 100 V during 24 h at 200 °C. Nevertheless, the leakage current density was considerably increased and the nonlinear features were also damaged.

These observations may be explained in view of the migration of species from depletion zones toward grain boundaries where they eventually react with negative species changing the voltage barrier characteristics (height and donor concentration). In SnO$_2$-based varistors, the higher thermal conductivity contributes to a better thermal dissipation reducing the local temperature.[22] Apparently the ionic diffusion process of SnO$_2$ varistors has a higher activation than that of ZnO-based varistors. The highly compact tetragonal structure of SnO$_2$ reduces the solid state diffusion of these ceramics under aging stress.[1,2]

IV. CONCLUSIONS

The electrical properties of varistors were damaged by means of dc voltage and current pulses. Before degradations,

for ZnO and SnO$_2$-based varistors, both thermionic and tunneling contributions for conduction were observed. Evidence that, after pulse degradation, current is mostly tunneling (for SnO$_2$ and ZnO varistors) was shown on the basis of capacitance versus frequency curves. For dc voltage degradation, ZnO-based varistors present mostly tunneling current in contrary with SnO$_2$-based varistors where thermionic and tunneling are in the same order of magnitude. The slow diffusion in SnO$_2$-based ceramics could be responsible of the low degradation observed.

ACKNOWLEDGMENTS

[1] M. A. Ramírez, W. Bassi, P. R. Bueno, E. Longo, and J. A. Varela, J. Phys. D **41**, 122002 (2008).

[2] M. A. Ramírez, M. Cilense, P. R. Bueno, E. Longo, and J. A. Varela, J. Phys. D **42**, 015503 (2009).

[3] K. Mukae, K. Tsuda, and I. Nagasawa, J. Appl. Phys. **50**, 4475 (1979).

[4] A. B. Glot and A. P. Zloblin, Neorg. Mater. **25**, 322 (1989) [Inorg. Mater. **25**, 274 (1989)].

[5] A. B. Glot, Y. N. Proshkin, and A. M. Nadzhafzade, in *Ceramics Today–Tomorrow's Ceramics*, Materials Science Monographs Vol. 66C, edited by P. Vincenzini (Elsevier, Amsterdam, 1991), p. 2171.

[6] A. B. Glot, in *Ceramic Materials Research Trends*, edited by P. B. Lin (Nova Science, Hauppauge, NY, 2007), pp. 227–273.

[7] P. R. Bueno, J. A. Varela, and E. Longo, J. Eur. Ceram. Soc. **28**, 505 (2008).

[8] A. B. Glot, A. V. Gaponov, and A. P. Sandoval-García, Physica B **405**, 705 (2010).

[9] C. R. Crowell and V. L. Rideout, Solid-State Electron. **12**, 89 (1969).

[10] E. H. Rhoederick and R. H. Williams, *Metal-Semiconductor Contacts*, 2nd ed. (Oxford Science, 1988).

[11] M. Matsuoka, in *Grain Boundary Phenomena in Electronic Ceramics*, Advances in Ceramics Vol. 1, edited by L. M. Levinson (American Ceramic Society, Columbus, OH, 1981), p. 290.

[12] S. A. Pianaro, P. R. Bueno, E. Longo, and J. A. Varela, Ceram. Int. **25**, 1 (1999).

[13] M. A. Ramírez, J. F. Fernández, M. de la Rubia, J. De Frutos, P. R. Bueno, E. Longo, and J. A. Varela, J. Mater. Sci.: Mater. Electron. **20**, 49 (2009).

[14] M. A. Ramírez, W. Bassi, R. Parra, P. R. Bueno, E. Longo, and J. A. Varela, J. Am. Ceram. Soc. **91**, 2402 (2008).

[15] M. A. Ponce, M. S. Castro, and C. M. Aldao, J. Mater. Sci.: Mater. Electron. **20**, 25 (2009).

[16] M. S. Castro and C. M. Aldao, Appl. Phys. Lett. **63**, 1077 (1993).

[17] P. R. Bueno, M. R. de Cassia-Santos, E. R. Leite, E. Longo, J. Bisquert, G. Garcia-Belmonte, and, F. Fabregat-Santiago, J. Appl. Phys. **88**, 6545 (2000).

[18] C. Malagú, M. C. Carotta, A. Giberti, V. Guidi, G. Martinelli, M. A. Ponce, M. S. Castro, and C. M. Aldao, Sens. Actuators B **136**, 230 (2009).

[19] E. R. Leite, A. M. Nascimento, P. R. Bueno, E. Longo, and J. A. Varela, J. Mater. Sci.: Mater. Electron. **10**, 321 (1999).

[20] R. Parra, M. A. Ponce, C. M. Aldao, and M. S. Castro, J. Eur. Ceram. Soc. **27**, 3907 (2007).

[21] C. Malagù, G. Martinelli, M. A. Ponce, and C. M. Aldao, Appl. Phys. Lett. **92**, 162104 (2008).

[22] P. R. Bueno, J. A. Varela, C. M. Barrado, E. Longo, and E. R. Leite, J. Am. Ceram. Soc. **88**, 2629 (2005).